An Adaptive Nonlinear Backstepping Control of DFIG Driven by Wind Turbine

Nihel KHEMIRI[1,4], Adel KHEDHER[2,5], Mohamed Faouzi MIMOUNI[3,4]

[1]Institut Supérieur des Sciences Appliquées et de Technologie de Gafsa, Cité Zarroug 2112 Gafsa
[2] Ecole Nationale d'Ingénieurs de Sousse, Cité Sahloul, 4054 Sousse
[3]Ecole Nationale d'Ingénieurs de Monastir, Cité Ibn-Aljazzar, 5000 Monastir
[4]Unité de recherche RME, INSAT, Zone urbaine Nord Tunis-Manar.
[5]Unité de recherche RELEV, ENIS, Sfax.
khemirin@yahoo.fr, Adel_kheder@yahoo.fr, Mfmimouni@enim.rnu.tn

Abstract:-In this paper we present a new control structure to extract the maximum power of a wind energy conversion system based on the double fed induction generator (DFIG). The proposed algorithm combines the nonlinear *Backstepping* approach and the field orientation scheme applied to control the rotor side converter (RSC) and the grid side converter (GSC) of the DFIG. The proposed strategy is asymptotically stable in the context of *Lyapunov* theory. Simulations results show interesting performances of the system in terms of the reference tracking stability and the robustness against parameters variations.

Key-words:-Double fed induction generator, nonlinear Backstepping control, *Lyapunov* approach, voltage oriented control.

1 Introduction

The wind turbines' variable speed operation has been used for many reasons. Among these are the decrease of the stresses on the mechanical structure, acoustic noises reduction and the possibility of active and reactive power control. Most of the major wind turbine manufacturers are developing new larger wind turbines in the 3–6 MW range [1]. These large wind turbines are all based on variable speed operation using a direct-driven synchronous generator, without gearbox, or a doubly fed induction generator with gearbox. The main advantage of the DFIG is that the power electronics equipment only carries a fraction of the total power (20–30%) [2,3]; this means that the losses in the power electronics converters, as well as the costs, are reduced.

DFIG controlled by field oriented control (FOC) technique, have been widely used in industrial applications for their low cost, high reliability, power efficiency and easy maintenance. The DFIG are difficult to control for several reasons:

i) Their dynamics are intrinsically non-linear and multivariable;

ii) Not all of the state variables and not all of the outputs to be controlled may be available for feedback.

The concept of field oriented control strategy can be viewed as a non linear feedback transformation that achieves torque-flux decoupling technique; various improvements have been made for this kind of control which is based, in fact, on proportional- integral (PI) controller used to control speed, flux and currents. In many motion control applications, using PI-controller presents suitable performances. However, when the machine parameters variations are registered, due especially to the natural phenomena machine effects (temperature, saturation and skin effect); the PI control performances may be seriously deteriorated. Since the backstepping theory is a systematic and recursive design methodology for non linear feedback control, the derived algorithm backstepping, replacing the PI controller into FOC structure, can give improved tracking response.

In the recent two decades, many modified non linear state feedback schemes such as input-output feedback linearization, passivity-based control and sliding mode control have been applied to more improve the induction generator control performances [4].

Especially in the pasts years, there has been tremendous amount of activity on a special control schemes know as "Backstepping" approaches. With these control algorithms, the feedback control laws are easily constructed and associated to *Lyapunov* functions.

In this paper, we have integrated the DFIG field oriented control on which the backstepping design will be applied. The idea of backstepping design is conducted to select recursively some appropriate functions of the state variables of the DFIG to be controlled. In this work, the speed and flux are assumed as pseudo-control inputs for lower dimension subsystems of the overall system [4].
This paper is organized as follows: In second section, we have presented a description of variable speed DFIG system. In third section we have modeled the wind generation system. We modeled in the first step the aerodynamic system and the DFIG in the second step. The fourth section is deals to the rotor side converter (RSC) control under backstepping. The fifth section is devoted to study the grid side converter (GSC) and DC-bus voltage using the FOC principle. In the last section, some simulation results are shown interesting obtained control performances of the DFIG in terms of the reference tracking ability and the robustness against parameters variations and we finish by a conclusion.

2 Variable-speed DFIG system

The studied system is composed by three-bladed rotor with a corresponding mechanical gearbox, a DFIG, two power converters, a DC-link capacitor, and a grid filter.
Including the DFIG, the individual components of electrical subsystem including a transmission line are modeled in the *dq*-synchronous reference frame. Wherein, *d*-axis is assumed to be aligned to stator flux, and the current coming out of the generator is considered positive.
The DFIG controllers utilize the concept of disconnection of the active and reactive power controls by transformation of the machine parameters into the *dq*-reference frame. Then, the active power can be controlled by influencing the *d*-axis rotor current while the reactive power can be controlled by *q*-axis rotor current.
The stator of the DFIG is connected to the grid. The rotor is driven by the wind generator whose is adjusted for optimum performance resulting in a variable speed operation.
When the machine is driven below synchronous speed, the output power from the stator is equal to the sum of the mechanical power from the wind turbine and the ac power injected into the rotor. In this case, GSC works as a rectifier and RSC works as an inverter. When the machine is driven above synchronous speed, power is recovered from the rotor with RSC working as a rectifier GSC working as an inverter. Control scheme include reactive and active power control is given by figure 1.

3 Modeling of the wind generation system

3.1 Modeling of the wind turbine

The aerodynamic power turbine P_t depends on the power coefficient C_p as follows:

$$P_t = \frac{1}{2} C_p(\lambda, \beta) \rho \pi R^2 \qquad (1)$$

Where ρ is the air density, R is the blade radius, β is the pitch angle and V is the linear wind speed.

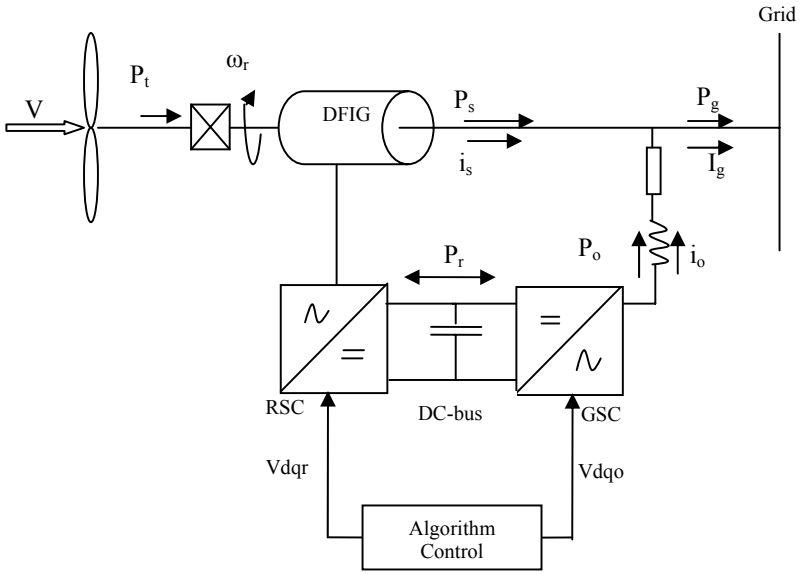

Figure 1: Wind energy conversion system

The turbine torque is given by:

$$T_t = \frac{P_t}{\Omega_t} \quad (2)$$

The turbine is normally coupled to the generator shaft through a gearbox whose gear ratio G is chosen in order to set the generator shaft speed within a desired speed range.

Neglecting the transmission losses, the torque T_g and the turbine speed [5], in turbine side of the gearbox Ω_t, are given by:

$$T_g = \frac{T_t}{G} \quad (3)$$

$$\Omega_t = \frac{\Omega}{G} \quad (4)$$

A wind turbine can only convert a part of the total of the captured wind power. The power coefficient depends on the pitch angle of the turbine and the ratio λ between the turbine angular speed Ω_t and the linear wind speed V. The coefficient in treated in some bibliographies [4]; the expression generally used is given by following:

$$C_p(\lambda,\beta) = c_1(c_2 g(\lambda,\beta) - c_3\beta - c_4)e^{-c_5 g(\lambda,\beta)} + c \quad (5)$$

where

$$g(\lambda,\beta) = \frac{1}{\lambda + 0.08\beta} - \frac{0.035}{\beta^3 + 1}$$

$C_i(i = 1,6)$ is given in Appendix.

The pitch angle β must be controlled to maintain the electric power constant. The characteristic resulting from measurements on a real wind shows that the pitch angle is fixed at 2 to maintain the power constant approximately at 660Kw.The regulation of the pitch is illustrated in figure 2.

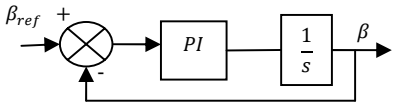

Figure 2: Regulation of the pitch angle by PI regulator

According eq. (1), the peak power for each wind speed occurs at the point where C_p is maximized. To maximize the generated power, it is therefore desirable for the generator to have a power characteristic that will follow the maximum C_{p_max} line. The action of the speed controller must achieve two tasks [6]:

- It must control the mechanical speed Ω in order to yet a speed reference Ω_c .
- It must attenuate the action of the aerodynamic torque, which is an input disturbance

The simplified representation in the form of diagram blocks is given by figure 3. If the wind speed is measured and the mechanical characteristics of the wind turbine are known, it is possible to deduce in real time the optimal mechanical power which can be generated using the maximum power point tracking (MPPT). The optimal mechanical power and the optimal mechanical torque can be expressed as:

$$P_{mec-opt} = \frac{1}{2}\rho\pi R^5 C_{pmax}\frac{\Omega^3}{\lambda_{opt}^2}\frac{1}{G^3} \quad (6)$$

$$T_{mec-opt} = \frac{1}{2}\rho\pi R^5 C_{pmax}\frac{\Omega^2}{\lambda_{opt}^2}\frac{1}{G^2} \quad (7)$$

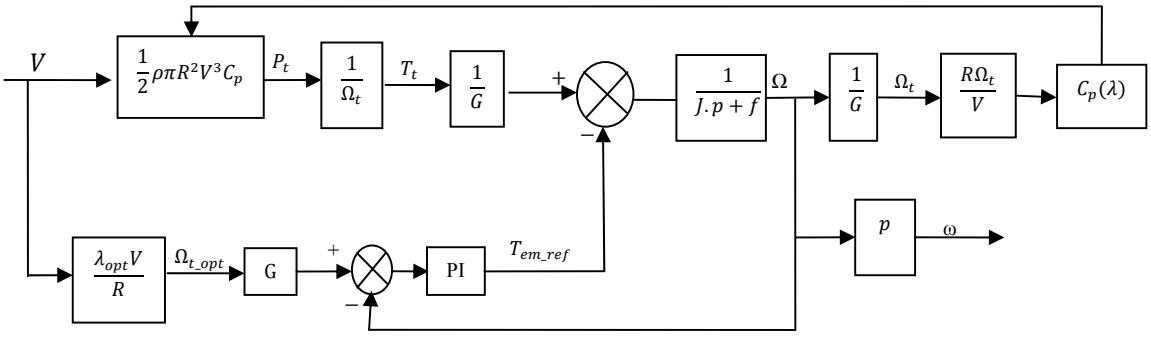

Figure 3: Dynamic model scheme

3.2 Modeling of the DFIG

The classical electrical equations of the DFIG in the Park frame are written as follows [7, 8]:

$$\begin{cases} \frac{d\Phi_{sd}}{dt} = V_{sd} - R_s i_{sd} + \Phi_{sq}\omega_s \\ \frac{d\Phi_{sq}}{dt} = V_{sq} - R_s i_{sq} - \Phi_{sd}\omega_s \\ \frac{d\Phi_{rd}}{dt} = V_{rd} - R_r i_{rd} + \Phi_{rq}\omega_r \\ \frac{d\Phi_{rq}}{dt} = V_{rq} - R_s i_{rq} - \Phi_{rd}\omega_r \\ \omega_r = \omega_s - \omega \end{cases} \quad (8)$$

The stator and rotor flux can be expressed as:

$$\begin{cases} \Phi_{sd} = L_s i_{sd} + M i_{rd} \\ \Phi_{sq} = L_s i_{sq} + M i_{rq} \\ \Phi_{rd} = L_r i_{rd} + M i_{sd} \\ \Phi_{rq} = L_r i_{rq} + M i_{sq} \end{cases} \quad (9)$$

Where i_{sd} , i_{sq} , i_{rd} and i_{rq} are respectively, the direct and quadrature stator and rotor currents
The stator and rotor active and reactive powers are given, respectively, by eq. (10) and eq. (11):

$$\begin{cases} P_s = \frac{3}{2}\left(V_{sd} i_{sd} + V_{sq} i_{sq}\right) \\ Q_s = \frac{3}{2}\left(V_{sq} i_{sd} - V_{sd} i_{sq}\right) \end{cases} \quad (10)$$

$$\begin{cases} P_r = \frac{3}{2}\left(V_{rd} i_{rd} + V_{rq} i_{rq}\right) \\ Q_r = \frac{3}{2}\left(V_{rq} i_{rd} - V_{rd} i_{rq}\right) \end{cases} \quad (11)$$

The electromagnetic torque is expressed as:

$$T_{em} = \frac{3}{2} p \frac{M}{L_s}\left(i_{rd}\Phi_{sq} - i_{rq}\Phi_{sd}\right) \quad (12)$$

4 Rotor side converter under non-linear backstepping control

The Backstepping control approach for the mechanical speed regulation and the flux generation can be better applied to replace the traditional non linear feedback (proportional-integral) PI control of the field oriented control technique for better performance.

4.1 Model description

In the stationary reference frame of the DFIG operate under FOC principle can be written under state form:

$$\begin{cases} \frac{di_{rd}}{dt} = \frac{1}{\sigma L_r} V_{rd} - \delta i_{rd} + \alpha R_s \Phi_{sd} + \beta V_{sd} + \omega_r i_{rq} \\ \frac{di_{rq}}{dt} = \frac{1}{\sigma L_r} V_{rq} - \gamma i_{rq} - \beta \omega_r \Phi_{sd} - \omega_r i_{rd} \\ \frac{d\Phi_{sd}}{dt} = -V_{sd} - \frac{R_s}{L_s}\Phi_{sd} + \frac{R_s M}{L_s} i_{rd} \\ \frac{d\Omega}{dt} = \frac{T_t}{J} - \frac{f}{J}\Omega - \frac{T_{em}}{J} \end{cases} \quad (13)$$

The electromagnetic torque is given by the following expression:

$$T_{em} = -\mu \Phi_{sd} i_{rq} \quad (14)$$

Where the state variables are the rotor currents (i_{rd}, i_{rq}), the stator flux (Φ_{sd}) and the mechanical speed Ω. The rotor voltages (V_{rd}, V_{rq}) are considered as the control variables. With the constants defined as:

$$\delta = \frac{R_r L_s^2 + M^2 R_s}{\sigma L_r L_s^2},\ \alpha = \frac{M}{\sigma L_r L_s^2},\ \beta = \frac{M}{\sigma L_r L_s},\ \gamma = \frac{R_r}{\sigma L_r},\ \mu = \frac{3}{2} p \frac{M}{L_s}$$

Accounting for eq. (14), the DFIG equations given by eq. (13) turn to be:

$$\begin{cases} \frac{d\Omega}{dt} = b_1 \\ \frac{d\Phi_{sd}}{dt} = b_2 \\ \frac{di_{rd}}{dt} = b_3 + \frac{1}{\sigma L_r} V_{rd} \\ \frac{di_{rq}}{dt} = b_4 + \frac{1}{\sigma L_r} V_{rq} \end{cases} \quad (15)$$

Where the different functions b_1 to b_4 are expressed as:

$$\begin{cases} b_1 = \frac{T_t}{J} - \frac{f}{J}\Omega + \frac{\mu}{J}\Phi_{sd} i_{rq} \\ b_2 = -V_{sd} - \frac{R_s}{L_s}\Phi_{sd} + \frac{R_s M}{L_s} i_{rd} \\ b_3 = -\delta i_{rd} + \alpha R_s \Phi_{sd} + \beta V_{sd} + \omega_r i_{rq} \\ b_4 = -\gamma i_{rq} - \beta \omega_r \Phi_{sd} - \omega_r i_{rd} \end{cases} \quad (16)$$

The DFIG system, given by eq.(15), will be approximately decomposed in two decoupled subsystems. Hence, they are considered (Ω, i_{rq}) as state variables and V_{rq} as input command for the first subsystem, while (Φ_{sd}, i_{rd}) as state variables and V_{rd} as input command for the second subsystem. The subsystem structure will be fully exploited in the backstepping control design as detailed in the next.

4.2 Control design

The basic idea of the Backstepping design is the use of the so-called "virtual control" to systematically decompose a complex nonlinear control design problem into simpler, smaller ones. Roughly speaking, Backstepping design is divided into various design steps [10]. In each step we essentially deal with an easier, single-input-single-output design problem, and each step provides a reference for the next design step. The overall stability and performance are achieved by a *Lyapunov* function for the whole system [11]. The synthesis of this control can be achieved in two steps.

(i) Step 1: Computation of the reference rotor currents

In the first step, it is necessary that the system follows given trajectory for each output variable [12]. To do so, a function $y_c = (\Omega_c, \Phi_c)$ is defined, where Ω_c and the Φ_c are the mechanical speed and stator flux references, respectively. The mechanical speed and stator flux tracking error e_1 and e_3 are defined by:

$$\begin{cases} e_1 = \Omega_c - \Omega \\ e_3 = \Phi_c - \Phi_{sd} \end{cases} \quad (17)$$

The derivative of Eq. (17) gives

$$\begin{cases} \dot{e}_1 = \dot{\Omega}_c - \dot{\Omega} \\ \dot{e}_3 = \dot{\Phi}_c - \dot{\Phi}_{sd} \end{cases} \quad (18)$$

Accounting for eq. (15), one can rewrite eq. (18) as follows:

$$\begin{cases} \dot{e}_1 = \dot{\Omega}_c - b_1 \\ \dot{e}_3 = \dot{\Phi}_c - b_2 \end{cases} \quad (19)$$

In order to check, let us the tracking performances choose the first *Lyapunov* [13] candidate function V_1 associated to the stator flux and mechanical speed errors, such us:

$$V_1 = \frac{1}{2}e_1^2 + \frac{1}{2}e_3^2 \quad (20)$$

Using eq. (19), the derivative of eq. (20) is written as follows:

$$\dot{V}_1 = e_1\left(\dot{\Omega}_c - b_1\right) + e_3\left(\dot{\Phi}_c - b_2\right) \quad (21)$$

This can be rewritten as follows:

$$\dot{V}_1 = -K_1 e_1^2 - K_3 e_3^2 \quad (22)$$

Where K_1, K_3 should be positive parameters [12], in order to guarantee a stable tracking, which gives:

$$\begin{cases} \dot{e}_1 = \dot{\Omega}_c - \dot{\Omega} = -K_1 e_1 \\ \dot{e}_3 = \dot{\Phi}_c - \dot{\Phi}_{sd} = -K_3 e_3 \end{cases} \quad (23)$$

Where:

$$\begin{cases} \dot{\Omega} = \dot{\Omega}_c + K_1 e_1 \\ \dot{\Phi}_{sd} = \dot{\Phi}_c + K_3 e_3 \end{cases} \quad (24)$$

Eq. (24) allows the synthesis of rotor current references, such as:

$$\begin{cases} \left(\Phi_{sd} i_{rq}\right)_c = \frac{J}{\mu}\left(\dot{\Omega}_c - \frac{T_t}{J} + \frac{f}{J}\Omega + K_1 e_1\right) \\ \left(R_s i_{rd}\right)_c = \frac{L_s}{M}\left(\dot{\Phi}_c + \frac{R_s}{L_s}\Phi_{sd} + K_3 e_3\right) \end{cases} \quad (25)$$

(ii) Step 2: Computation of the reference rotor voltages

In this step, an approach to achieve the current reference generated by the first step is proposed. Let us recall the current errors, such as:

$$\begin{cases} e_2 = \left(\Phi_{sd} i_{rq}\right)_c - \Phi_{sd} i_{rq} \\ e_4 = \left(R_s i_{rd}\right)_c - R_s i_{rd} \end{cases} \quad (26)$$

Accounting for eq. (25), eq. (26) turns to be:

$$\begin{cases} e_2 = \frac{J}{\mu}\left(\dot{\Omega}_{ref} - \frac{T_t}{J} + \frac{f}{J}\Omega + K_1 e_1\right) - \Phi \\ e_4 = \frac{L_s}{M}\left(\dot{\Phi}_{sd-ref} + \frac{R_s}{L_s}\Phi_{sd} + K_3 e_3\right) - \end{cases} \quad (27)$$

The time derivative of eq. (26) yields:

$$\begin{cases} \dot{e}_2 = \left(\dot{\Phi_{sd}} i_{rq}\right)_c - \left(\Phi_{sd} \dot{i_{rq}}\right) = A_1 - \frac{1}{\sigma L_r}\Phi \\ \dot{e}_4 = \left(R_s \dot{i_{rd}}\right)_c - \left(R_s \dot{i_{rd}}\right) = A_2 - \frac{R_s}{\sigma L_r} V_{rd} \end{cases} \quad (28)$$

Where A_1, A_2 are known signals that can be used in the control, and their expressions are as follows:

$$A_1 = f_a \ddot{\Omega}_{ref} - K_1^2 f_b e_1 + K_1 e_2 + f_c C_t - f_d \Omega + \left(f_e + f_f + f_h\right)\Phi_{sd} i_{rq} - f_g i_{rd} i_{rq} + \omega_r \Phi_{sd} i_{rd} \quad (29)$$

$$A_2 = -f_j K_3^2 e_3 + K_3 e_4 + f_j \ddot{\Phi}_{sd-ref} - f_l \Phi_{sd} + f_k i_{rd} - R_s \omega_r i_{rq}$$

With

$$f_a = f_b = \frac{JL_s}{3M}, f_c = \frac{fL_s}{3MJ}, f_d = \frac{f^2 L_s}{3JM}, f_e = \frac{f}{J}, f_f = \frac{R_s}{L_s},$$

$$f_g = \frac{R_s M}{L_s}, f_h = \frac{R_r}{\sigma L_r}, f_i = \frac{M}{\sigma L_s L_r}, f_j = \frac{L_s}{M},$$

$$f_k = \frac{R_s^2}{L_s} + \frac{R_s R_r L_s^2 + M^2 R_s^2}{\sigma L_r L_s^2}, f_l = \frac{R_s^2}{ML_s} + \frac{MR_s^2}{\sigma L_r L_s^2}, f_m = \frac{R_s}{M}$$

One can notice that eq. (28) include the system inputs: the rotor voltage. These could be find out through the definition of a new *Lyapunov* function based on the

(30)

errors of the speed, of the stator flux and the rotor currents [1], such that:

$$V_2 = \frac{1}{2}(e_1^2 + e_2^2 + e_3^2 + e_4^2)$$

The derivative of Eq. (30) is given by:

$$\dot{V}_2 = e_1\dot{e}_1 + e_2\dot{e}_2 + e_3\dot{e}_3 + e_4\dot{e}_4 \quad (31)$$

By setting eq. (25) in eq. (30), one can obtain:

$$\dot{V}_2 = -K_1e_1^2 - K_2e_2^2 - K_3e_3^2 - K_4e_4^2 + e_2\left(\frac{\mu}{J}e_1 + A_1 - \frac{1}{\sigma L_r}\Phi_{sd}V_{rq} + K_2e_2\right) + e_4\left(\frac{M}{L_s}e_3 + A_2 - \frac{R_s}{\sigma L_r}V_{rd} + K_4e_4\right) \quad (32)$$

The derivative of the complete *Lyapunov* function eq. (32) can be negative definite, if the quantities between parentheses in eq. (32), would be chosen equal to zero.

$$\begin{cases} \frac{\mu}{J}e_1 + A_1 - \frac{1}{\sigma L_r}\Phi_{sd}V_{rq} + K_2e_2 = 0 \\ \frac{M}{L_s}e_3 + A_2 - \frac{R_s}{\sigma L_r}V_{rd} + K_4e_4 = 0 \end{cases} \quad (33)$$

The rotor voltages then deduced as follows:

$$\begin{cases} V_{rd} = \frac{\sigma L_r}{R_s}\left[\frac{M}{L_s}e_3 + A_2 + K_4e_4\right] \\ V_{rq} = \frac{\sigma L_r}{\Phi_{sd}}\left[\frac{\mu}{J}e_1 + A_1 + K_2e_2\right] \end{cases} \quad (34)$$

Where K_2 and K_4 are positive parameters selected to guarantee a faster dynamic of the rotor current those of the stator flux and speed.

From the above we can obtain the control laws as

$$\dot{V}_2 = -K_1e_1^2 - K_2e_2^2 - K_3e_3^2 - K_4e_4^2 \leq 0 \quad (35)$$

The bloc diagram of the proposed Backstepping control scheme is illustrated by Figure 4.

The blocks $(i_{rd})_c$ −Computation and $(i_{rq})_c$ −Computation provide respectively the rotor currents references components via the stator flux and speed feedback controls.

According to eq. (25), these currents components characterize the so-called fictive input commands. The voltage command are generated from the feedback control of the rotor current components are given by the two blocks V_{rd}-Computation and V_{rq}-Computation which are implemented from Eq. (34). So, we cannot that the four calculations replace naturally the classical PI-controllers utilized into the field control of a DFIG.

As indicate in figure 4, we use two blocks to estimate the mechanical speed and stator flux.

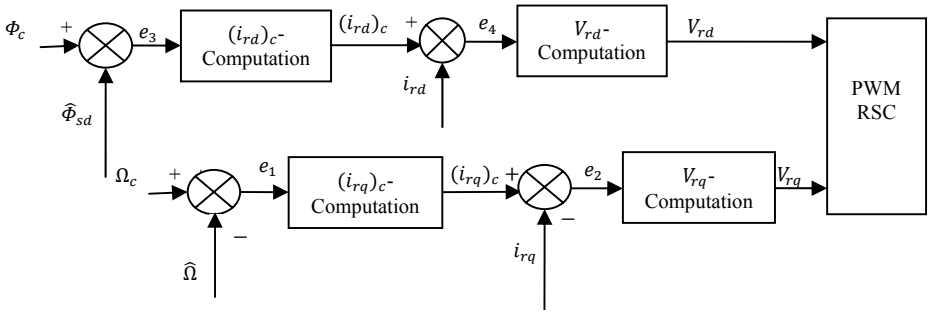

Figure 4: Block Diagram of the proposed sensorless backstepping FOC for a DFIG

4.3 Stator flux and mechanical speed estimator

The stator flux has been estimated using the simplified DFIG model obtained after the application of the field oriented control principle. Where much simplification is gained by the fact that $\Phi_{sd} = 0$. This allows estimation of the stator flux vector is given by Figure 5.

According to the fifth equation from Eq. (8), it is possible to compute $\widehat{\omega}$ as follows:

$$\widehat{\omega} = \omega_s - \widehat{\omega}_r = \omega_s - \frac{M}{\tau_r}\frac{i_{sq}}{\Phi_{sd}} \quad (36)$$

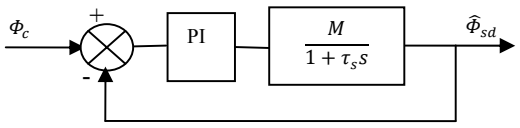

Figure 5. Stator flux estimator

5 Grid side converter and DC-bus voltage control

5.1 Grid Side Converter control

In order to keep constant DC voltage to supply the rotor side converter and realize a variable speed control, a rectifier interfacing the grid is needed. By sub synchronous rotor angular speeds, a part of the aerodynamic energy captured by the turbine is used via the grid side converter to brake the generator. In this mode the converter works as rectifier. By super synchronous rotor angular speeds, on the contrary, all the converted electric power is transferred into the grid. The grid side converter acts then as inverter. The possibility to drive the induction generator in this two operating conditions forces to design the grid side converter as a bidirectional one.

Task of the grid side converter during normal operations is to transform a three-phase voltage into a DC voltage. This one has to be kept to a constant value [3].
The control scheme that achieves this task is based on the error between the reference and the actual DC voltage. A PI controller applied to this measured error provides the current amplitude reference on the AC side. This is used to determine the modulating waves for the converter, which is acted as a boost rectifier. This way the currents on the rotor side can be reduced, while increasing the voltage.
The converter with dimensions grid is an inverter of tension (V_{od}, V_{oq}) and the variables of control are the output GSC currents (i_{od}, i_{oq}). With an aim independently of controlling the active and reactive powers system forwarded towards the network, choosing us to oriented the network voltage according to the Park direct axis [2]:

$$\begin{cases} V_{Rd} = V_R \\ V_{Rq} = 0 \end{cases} \tag{37}$$

By supposing that the assumptions of orientation of the vector grid voltage are satisfied, the expressions of the active power and of the reactive power become:

$$\begin{cases} P_0 = \frac{3}{2} V_R i_{od} \\ Q_0 = -\frac{3}{2} V_R i_{oq} \end{cases} \tag{38}$$

In order to obtain the maximum active power forwarded towards the grid, it will be supposed that the reactive power of reference is null ($Q_{ref} = 0$). So we obtain a null current of reference i_{0q-ref} [6]:

$$i_{oq-ref} = \frac{P_{0-ref} V_{Rd} + Q_{0-ref} V_{Rq}}{\frac{3}{2}\left(V_{Rd}^2 + V_{Rq}^2\right)} \tag{39}$$

5.2 DC-bus Voltage Control

On the level of the continuous bus, energy is written:

$$W_{dc} = \int_0^t P_{dc} dt = \frac{1}{2} C V_{dc}^2 \tag{40}$$

The dc-power is given by derivative of energy equation [11]:

$$P_{dc} = \frac{dW_{dc}}{dt} = C V_{dc} \frac{dV_{dc}}{dt} \tag{41}$$

The dc-bus power assessment is given by:

$$P_{dc} = P_{em} - P_{js} - P_{jr} - P_s - P_o \tag{42}$$

Knowing P_r the rotor power, P_s the stator power, that exchanged by the, the stators and rotor coppers losses P_{js} and P_{jr}. Then, the V_{dc} makes it possible to control the current i_o on the GSC output.

$$V_{dc} \frac{dV_{dc}}{dt} = A - B i_{od} \tag{43}$$

With:

$$\begin{cases} A = \frac{P_{em} - P_{jr} - P_{js} - P_s}{C} \\ B = \frac{V_R}{C} \end{cases} \tag{44}$$

The DC voltage link is controlled by the PI- regulator, as illustrated in Figure 6.

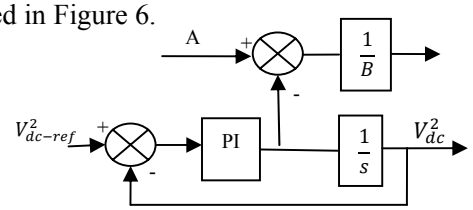

Figure 6: DC-voltage regulation loop

5.3 Stability Analysis

To prove the convergence properties and stability of the overall closed loop system, we will prove that all the signals of the states are bounded and all tracking errors and all estimation and observation errors converge to zero asymptotically. For that, the proof is established for adaptative backstepping controller via *Barbalat*'s Lemma [4] using the *Lyapunov* candidate function. For that, we have to prove

(45)

$$e_1, e_2, e_3, e_4 \, \mathcal{E} \, \mathcal{L}_\infty \cap \mathcal{L}_2, \dot{e}_1, \dot{e}_2, \dot{e}_3, \dot{e}_4 \mathcal{E} \, \mathcal{L}_\infty$$

These conditions imply, via Barbalat's Lemma that the closed-loop is stable and that e_1, e_2, e_3 and e_4 all converge to zero.
We begin with the facts that V_2 is positive definite, and $\dot{V}_2$ is semi-negative definite, thus all the error signals e_1, e_2, e_3 and e_4 are pounded. With our assumptions on the reference signals Ω_c, Φ_c, we get that the signals A_1 and A_2 are bounded. Therefore by eq. (19) and eq. (28), we know that $\dot{e_1}, \dot{e_2}, \dot{e_3}$ and $\dot{e_4}$ are bounded. Now, what left is to prove $e_1, e_2, e_3, e_4 \, \mathcal{E} \, \mathcal{L}_2$.
By the eq. (20), eq. (22), eq. (20) and eq. (35) we get

$$V_1 \dot{V_1} \leq 0 \text{ and } V_2 \dot{V_2} \leq 0 \qquad (46)$$

6 Simulations results

The proposed DFIG control has been simulated using Matlab/Simulink. DFIG parameters are those in appendix. The parameters K_1, K_2, K_3 and K_4 of the backstepping control are chosen as follows: $K_1 = 2800$, $K_2 = 1200$, $K_3 = 0.001$ and $K_4 = 9000$ to satisfy convergence condition.

We have made three simulations:

1) In the first case, we present the DFIG response under nonlinear backstepping control. Figure 7 illustrates the speed, the electromagnetic torque and the flux variations. Figure 8 illustrates the three phase stator, rotor and grid currents and the stator, the rotor and the grid powers variations.

2) In the second case we have studied the dynamic performances of the proposed control strategy. The corresponding results are given by Figure 9 and Figure 10. By these figures we illustrate the speed and the stator flux variations. We introduce a sudden increase and decrease of the reference speed and the sudden increase and decrease of the reference stator flux.

3) In the third case, we have studied the stability of the system. The study is based on the illustration of the *Lyapunov* candidate function and its derivative. The corresponding results are illustrated by Figure 11.

The responses of the DFIG under Backstepping control strategy is shown in Figure 7 and Figure 8. The illustrated variables are:

- Figure 7a shows that the mechanical speed converges perfectly to their reference value coming from the control in MPPT operation conditions of the turbine.
- Figure 7b shows that the dq-axis stator flux components. One can notice that the q-axis stator flux is almost null and the d-axis one is equal to the nominal value.
- Figure 7c shows that the dq-axis rotor flux components. We remark that the rotor flux appears a oscillation in transient state.
- Figure 7d shows that the electromagnetic torque when it takes the nominal value in permanent state.
- Figure 7e shows that estimated and reference stator flux which is a pulse of 3 Wb. One can notice the high performance of the stator flux loop.
- Figure 8a and Figure 8b shows respectively the zoom of stator and rotor current. These figures represent a good pursuit.
- From Figure 8c, one remark that the grid current in the three phase's network constitute a balanced system of frequency 50Hz.
- Figure 8d shows that only third of the total power injected to the grid pass by the power converter. As well the grid power P_g is equal to the sum of the stator power P_s and the output power of the GSC P_0.

Figure 9 and Figure 10 shows the satisfactory performances respectively of the speed and stator flux tracking. Although the speed reference suddenly increased from their nominal values to 202rad/s at t=2s and decreases to 132rad/s at t=3.5s, the stator flux reference increases from 3Wb to 4.5Wb at t=2s, and decreases to 1.5Wb at=3.5s. We can see that the actual speed and stator flux follows well the variations of its reference.
We can find also, that the speed error and the stator flux error given by e_1 and e_3. We can remark that the increase of the mechanical speed reference Ω_c and the stator flux reference Φ_c, respectively, amplifies the static error and their decreases (Ω_c and Φ_c), down the static error and it appears a small static error in steady condition with respect to nominal case.
Thus, the simulation results confirm the robustness of the proposed scheme against the reference speed and stator flux variations.

To prove the stability of the overall system, we will prove that
$V_1\dot{V_1} \leq 0$ and $V_2\dot{V_2} \leq 0$ shown in Figure 11.

7 Conclusion

This work described a control approach applied on DFIG driven by wind turbine to extract the maximum power from the wind will to the grid. The system uses two rotor power converters linked by a DC voltage which allow the power energy transient between the grid and the wind energy conversion system. In the first phase, we used the adaptive non linear backsteppig control in the RSC. In the second phase, we have used the oriented network voltage principle to control the GSC. Simulations results are shown interesting obtained control performances of the DFIG. Global asymptotic stability was achieved via the *Lyapunov* stability analysis. The obtained results show that the robustness of Backstepping nonlinear control against parameters variations.

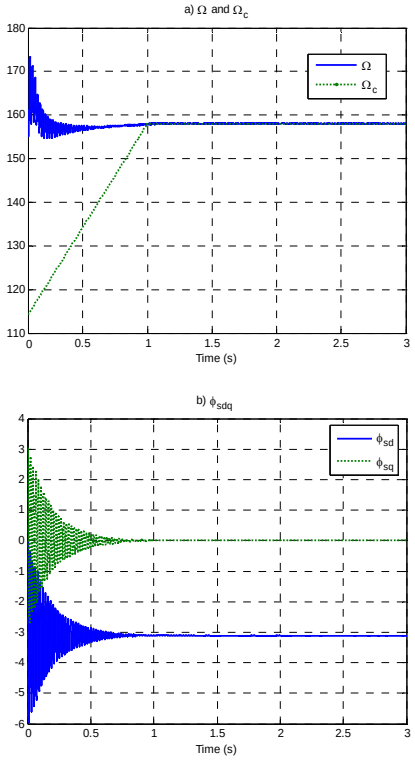

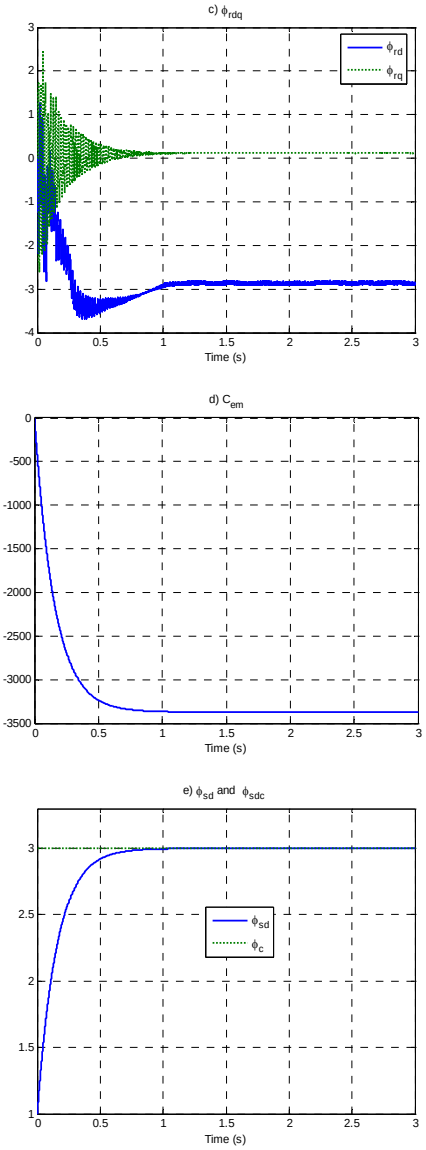

Figure 7: Response of the DFIG under Backstepping control strategy (Speed, electromagnetic torque, and Stator and rotor flux)

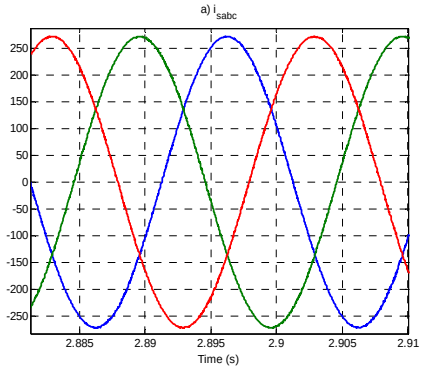

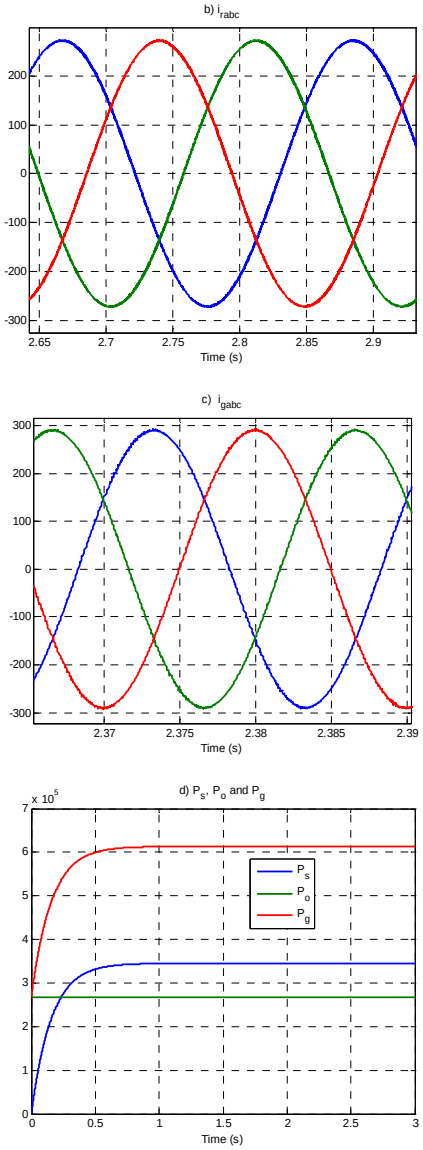

Figure 8: Responses of the DFIG under Backstepping control strategy (Stator, rotor and grid currents and powers)

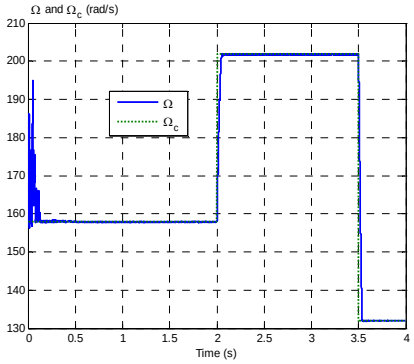

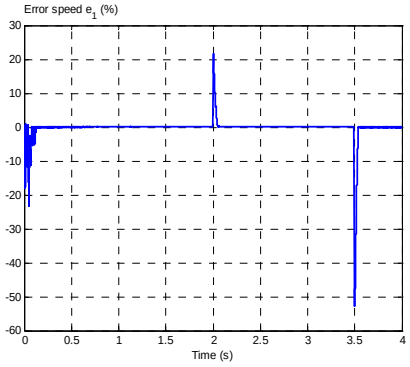

Figure 9: Dynamic response of the DFIG under backstepping control with speed variations

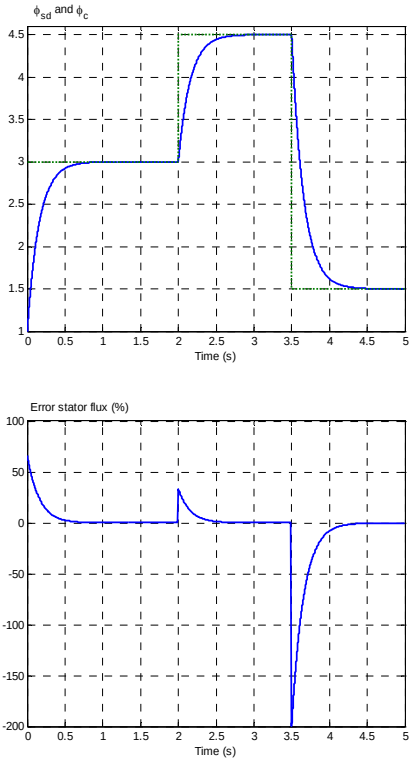

Figure 10: Dynamic response of the DFIG under backstepping control with stator flux variations

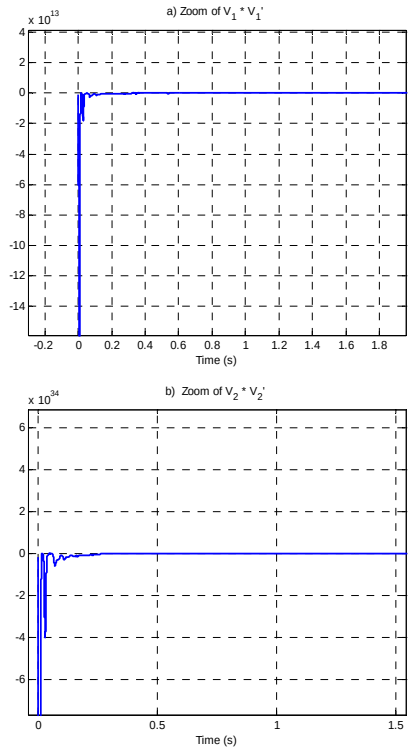

Figure 11: Lyapunov candidate function variations

8 References

[1] R.R. Joshi, R.A. Gupta and A.K. Wadhwani, Adaptive Backstepping controller design and implementation for a matrix-converter-based IM drive system, *Journal of Theoretical and Applied Information Technology*, 2007 JATIT.

[2] Jihène Ben Alaya, Adel Khedher and Mohamed Faouzi Mimouni, DTC and Nonlinear Vector Control Strategies Applied to the DFIG operated at Variable Speed, *WSEAS Transactions on environment and development*, vol. 6, N° 11, November 2010, pp. 744-753.

[3] J. Ben Alaya, A. Khedher and M.F. Mimouni, Variable Speed vector Control Strategy of the Double fed Induction Generator Integrated in Electrical Grid, *in CD-ROM of Inter. Conf. on Ecologic Vehicles and Renewable Energy (EVER'08),* Monaco, France, March/April 2008.

[4] R. Abdessemed, A.L.Nemmour, F.Mehazzem, A. Khezzar, M.Hacil and L. Louze, Advanced Backstepping controller for induction generator using multi-scalar machine model for wind power purposes, *Renewable Energy journal homepage (ELSEVIER)*, 18 February 2010.

[5] F. Mehazzem, A. Reama and H. Benalla, Sensorless nonlinear adaptive backstepping control of induction motor, *ICGST- ACSE journal*, vol. 8, Issue III, January 2009.

[6] K. Hee-Sang, Y. Gi-Gab, K. Nam-Ho and H. Won-Pyo, Modeling and control of DFIG-based variable-speed wind-turbine, *Electric Power Systems Research,* vol.78,n°16, pp. 1841–1849, July 2008.

[7] A. Tapia, G. Tapia, J. Ostolaza and J. saenz, Modeling and control of a wind turbine driven doubly fed induction generator, *IEEE Trans. On Energy Conversion*, vol. 18, n°2,pp. 194-204, June 2003.

[8] P. Andreas, H. Lennart and T. Torbjorn, Evaluation of Current Control Methods for Wind Turbines Using Double-Fed Induction Machines, *IEEE Trans. on Power Electronics*, Vol. 20, n°1, pp 227-235, January 2005.

[9] N. Khemiri, A. Khedher and M.F. Mimouni "Steady-state performances analysis of wind turbine using DFIG drive connected to grid, in CD-ROM of *International Conference JTEA'10,* Hammamet-Tunisia, 26-28 Mars 2010

[10] A. Laoufi, A. Hazzab, I.K. Bousserhane and M. Rahli "Direct Field-Oriented control using Backstepping technique for Induction Motor speed control, *International Journal of Applied Engineering Research* , vol. 1, n°1,pp. 37-50, 2006.

[11] H. Tan and J. Chang, Field orientation and adaptative Backstepping for induction motor control, *Thirty-Fourth IAS Annual Meeting, IEEE Industry Applications Conference*, vol. 4, pp: 2357-2363, 3-7 October1999.

[12] R.Trabelsi, A.Khedher, M.F. Mimouni, F.M'Sahli and A. Masmoudi "Rotor flux estimation based on nonlinear feedback integrator for backstepping-controlled induction motor drives, *Electromotion Journal 17*, 2010, pp:163-172.

[13] R.Trabelsi,A.Khedher, M.F. Mimouni and F.M'Sahli, An Adaptive Backstepping Observer for on-line rotor resistance adaptation, *International Journal IJ-STA,* Volume 4, n°1, July 2010, pp.1246-1267.

Appendix: Induction generator data

Rated power	660Kw
Rated stator voltage	400/690V
Nominal frequency	50 Hz
Number of pole pairs	n_p=2
Rotor resistance	$R_r = 0.0238\Omega$
Stator resistance	$R_s = 0.0146\Omega$
Stator inductance	$L_s = 0.0306H$
Rotor inductance	$L_r = 0.0303$
Mutual inductance	M=0.0299H

Appendix: wind turbine data

Rated power	660Kw
Blade Radius	R = 21.165 m
Power coefficient	C_{pmax} = 0.42
Optimal relative wind speed	λ_{opt}= 9
Mechanical speed multiplier	G=39
Moment of inertia	J=28 Kg.m^2
Damping coefficient	f= 0.01

Appendix: Power coefficient constants

$c_1 = 0.5109$	$c_4 = 5$
$c_2 = 116$	$c_5 = 21$
$c_3 = 0.4$	$c_6 = 0.0068$

List of Symbols

P_t : Wind turbine power (aerodynamic power)
T_t : Wind turbine torque (Nm),
V : Wind speed (m/s)
R : Blade radius (m)
ρ : Air density
β : Pitch angle
p: Number of pair poles
C_p : Power coefficient
Ω_t: Wind turbine angular speed (shaft speed) (rad/s)
Ω: Mechanical speed (rad/s)
λ : Relative wind speed
λ_{opt} : Optimal relative wind speed
G: Mechanical speed multiplier (gearbox)
J: Moment of inertia
*f: D*amping coefficient
C_t : Wind turbine torque (Nm)
T_{em} : Electromagnetic torque (Nm)
V_s, V_r Stator and rotor voltage (V)
i_{sd}, i_{sq} Direct and quadrature component of the stator currents (A)
i_{rd}, i_{rq} Direct and quadrature component of the rotor currents (A)